COMMUNICATION

Targeted detection method for locus-specific m⁶A modifications in low-abundance transcripts based on chemical conversion

Ting Liu,[†a] Xin Fang,[†a] Yue Lu,[a] Xiumin Liu,[a] Ruiqi Zhao,[*a] Xiang Zhou [ID] [ab] and Xiaocheng Weng [ID] [*ab]

In this study, we developed a method for locus-specific m⁶A detection, which employs sodium nitrite and glyoxal-based chemical conversion with probe hybridization. This approach enables highly sensitive detection of target m⁶A sites even in low-abundance transcripts.

Since the discovery of pseudouridine in 1957,[1] over 170 types of RNA modifications have been identified.[2] Among these, N⁶-methyladenosine (m⁶A) stands out as one of the most abundant endogenous chemical modifications in eukaryotic mRNAs. Its dynamic regulation is orchestrated by three classes of evolutionarily conserved enzymes: "writers" (*e.g.*, METTL3 and METTL14[3]) that catalyze methylation; "erasers" (*e.g.*, FTO[4] and ALKBH5[5]) responsible for demethylation; and "readers" (*e.g.*, the YTH domain family[6]) which recognize m⁶A sites. These enzymes regulate m⁶A dynamics, driving the developement of activity detection, which have enabled applications in single-cell imaging and cancer diagnosis.[7,8] The m⁶A modification directly influences RNA and regulates diverse developmental and cellular processes. Notably, m⁶A levels are closely linked to the pathogenesis of numerous diseases, positioning m⁶A as a potential diagnostic biomarker and therapeutic target.[9–12] Consequently, the precise detection of m⁶A sites is critically important for both fundamental research and biomedical applications.

The first transcriptome-wide m⁶A mapping was achieved in 2012 using m⁶A-seq[13] and MeRIP-seq.[14] Subsequent refinements integrated UV crosslinking into antibody-based approaches, such as miCLIP,[15] PA-m⁶A-seq[16] and m6ACE-seq[17] to achieve higher resolution. However, these methods remain constrained by relatively low resolution and high RNA input requirements. To overcome these limitations, various antibody-independent

strategies have emerged. Methods such as m⁶A-label-seq,[18] m⁶A-SAC-seq,[19] MePMe-seq,[20] m⁶A-SEAL-seq,[21] MAZTER-seq[22] and m⁶A-REF-seq[23] achieved single-base resolution through metabolic labeling or m⁶A-sensitive enzymes. In parallel, techniques including the DART-seq,[24] eTAM-seq,[25] GLORI,[26,27] and CAM-seq[28] employ enzymatic or chemical conversion to induce selective deamination, enabling transcriptome-wide m⁶A profiling by high-throughput sequencing. While these methods enable transcriptome-wide m⁶A profiling, clinical diagnostics increasingly require locus-specific detection method. The SCARLET method first validated single-nucleotide m⁶A detection in 2013.[29] Subsequent techniques, such as SELECT,[30] LEAD-m⁶A-seq,[31] E-IEXPAR[32] and Rol-LAMP[33] exploit the ability of m⁶A to block polymerase or ligase extension, converting modification status into quantifiable amplification signal. Other methods like TARS,[34] m⁶AISH-PLA[35] and m6A-PHPEA[36] visualize locus-specific m⁶A sites in cells *via* fluorescence labeling. Advanced m⁶A detection methods based on single-molecule counting have also been developed (see reviews for details).[37] However, these methods mainly rely on the enzymes selectivity for m⁶A sites, which generally leads to poor selectivity compared to chemical approaches. Consequently, new detection methods are still needed to accurately identify m⁶A sites, particularly in low-abundance transcripts.

To advance locus-specific m⁶A detection, we develop a targeted method that integrates chemical conversion with ligation-mediated qPCR amplification, enabling sensitive detection with minimal sample input. The experimental workflow comprises: (1) chemical conversion of unmodified adenosines using sodium nitrite and glyoxal; (2) reverse transcription to generate cDNA; and (3) PCR amplification to enhance signals from low-abundance transcripts. Complementary UP and DOWN probes, flanking the target site, are hybridized to the cDNA. If the adenosine is m⁶A-modified, it resists chemical conversion, enabling efficient probe ligation *via* the primer sequences at their ends and subsequent amplification. Conversely, an unmodified adenosine (A) is chemically converted, preventing ligation and reducing product yield. This difference is quantified by a

[a] College of Chemistry and Molecular Sciences, State Key Laboratory of Metabolism and Regulation in Complex Organisms, Wuhan University, Wuhan, Hubei, 430072, China. E-mail: rqzhao@whu.edu.cn, xcweng@whu.edu.cn

[b] Wuhan TaiKang Center for Life and Medical Sciences, Wuhan University, Wuhan, Hubei, 430071, P. R. China
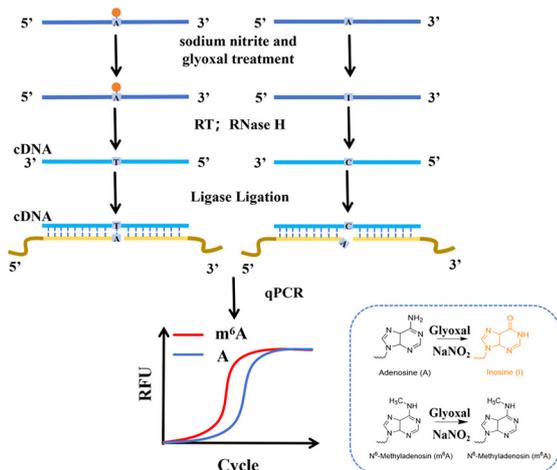
† These authors contributed equally.

Fig. 1 Schematic diagram of the locus-specific m^{6}A detection workflow based on qPCR. Glyoxal and nitrite mediate the deamination of adenosine (A) to Inosine (I). The designed probes ligate only upon recognition of unconverted sites after RT, generating ligation-dependent signal differentiation.

shift in the qPCR cycle threshold (C_t), enabling sensitive and single-base resolution detection of m^{6}A (Fig. 1). If there are varying degrees of modification at this site, it can still be confirmed that there is some modification by comparing the C_t values before and after demethylation.

We first validated the method using synthetic oligonucleotides (45 DNA T and 45 DNA C, Table S1), which mimic cDNA from reverse-transcribed RNA treated with sodium nitrite and glyoxal, containing either m^{6}A (45 DNA T) or unmodified A (45 DNA C). Ligation efficiency was compared under two base-pairing modes (A–T and G–C), corresponding to target sites with m^{6}A (read as A) or converted A (read as G) (Fig. S1A). Corresponding upstream probes (ending in A or G) and a downstream probe were designed to flank the target site. qPCR analysis revealed distinct ligation products between 45 DNA T and 45 DNA C under both pairing modes (Fig. S1B and C), confirming that the ligation-based qPCR strategy effectively discriminates m^{6}A from unmodified A. As the A–T mode showed a more pronounced difference in product yield, it was selected for all subsequent experiments.

To assess the impact of terminal base mismatches on ligation efficiency, a series of probes were designed with variations at terminal or penultimate positions: UP probes with different terminal bases (UP-A, UP-G, UP-T, UP-C) or penultimate-base substitutions (UP-2G, UP-2A, UP-2T, UP-2C), and DOWN probes with varying terminal bases (DOWN-C, DOWN-A, DOWN-T, DOWN-G) (sequences in Table S1). Correctly matched probes (UP-A, UP-G, UP-2G, and DOWN-C) yielded the highest ligation efficiency, whereas all mismatched combinations substantially reduced product formation (Fig. S2). We then optimized the ligation step by comparing Hifi Taq, SplintR, and T4 DNA ligases. Reaction conditions—including enzyme concentration (2, 5, 10, 15, and 25 U), temperature (40, 50, 60, and 70 °C), and time (15, 30, 45, and 60 min) were systematically screened (Fig. S3 and S4). Initial validation showed that T4 DNA Ligase

had lower efficiency than the other two enzymes (Fig. S3). Further optimization revealed that HiFi Taq DNA Ligase performs better at lower concentrations. The reduced sequence complexity after chemical treatment allowed higher ligation temperatures, promoting more accurate hybridization. HiFi Taq DNA Ligase achieved maximal product yield at 70 °C, making it the optimal choice (Fig. S4). Based on product yield and discrimination between matched and mismatched probes, 2 U Hifi Taq DNA Ligase at 70 °C for 30 min was selected as optimal. Furthermore, placing the adenosine (A) at the 3′ terminus of the UP probe proved more efficient than at the 5′ end of the DOWN probe (Fig. S3).

Next, we determined the detection limit using synthetic RNA oligonucleotides (45 RNA A and 45 RNA m^{6}A, Table S1). With 14 fmol of input RNA, the cycle-threshold difference (ΔC_t) between m^{6}A and A reached 6.11 cycles, corresponding to 69.07-fold selectivity (Fig. 2A). However, detection became unreliable below 0.14 fmol input RNA (Fig. 2B). Introducing a pre-amplification step (35-cycle PCR of cDNA prior to ligation) restored m^{6}A detection at 0.14 fmol, yielding a ΔC_t of 4.1 cycles (Fig. 2C). Further dilution experiments showed the method could distinguish m^{6}A from A at inputs as low as 0.0007 fmol (Fig. 2D)—significantly below the 0.25 fmol required by SELECT.[30] These results demonstrate that our approach enables highly sensitive, locus-specific m^{6}A detection, making it suitable for analyzing low-abundance transcripts in limited samples.

After method validation and optimization, we assessed its performance in biological samples. Using FTO-mediated demethylation to convert m^{6}A to A at specific sites, we directly compared modification states before and after treatment within the same sample (Fig. S7). If this site has certain m^{6}A modifications, after FTO treatment, the m^{6}A/A ratio will show changes. Through chemical treatment, these changes will be amplified, thereby detecting that this site has certain m6A modifications. After
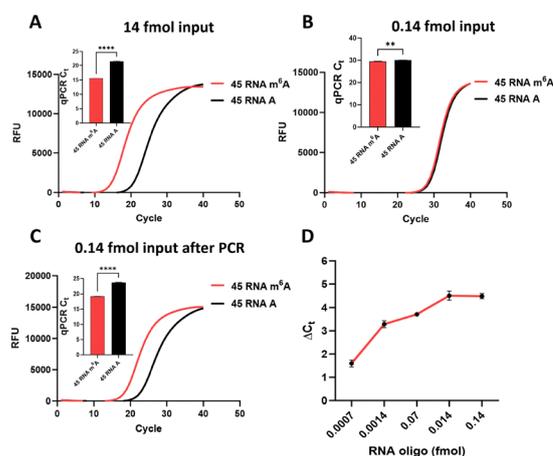

Fig. 2 Evaluation of the method's detection limit using RNA oligonucleotides. Real-time fluorescence amplification curves of the 14 fmol (A) and 0.14 fmol (B) RNA oligo input. (C) Real-time fluorescence amplification curves of the 0.14 fmol RNA oligo input after PCR amplification. (D) Detection limit using RNA oligo below 0.14 fmol. Error bars indicate mean ± s.d. for three technical replicates. *$P < 0.05$; **$P < 0.01$; ***$P < 0.001$; ns, non-significant by t-test (two-tailed).
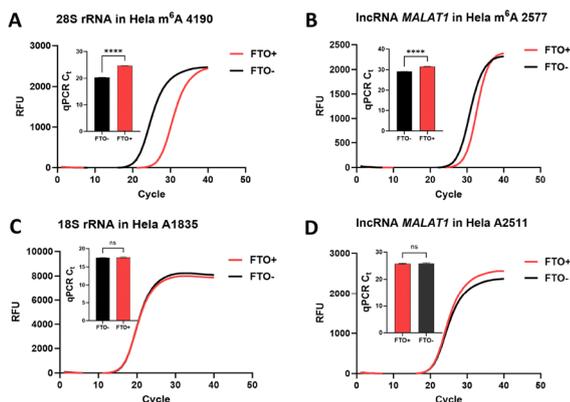
Fig. 3 Validation of known m⁶A sites and control A sites on rRNA and lncRNA through FTO-mediated demethylation. Detection results of m⁶A sites (A), (B) and A sites (C), (D) on rRNA and lncRNA presented by real-time amplification curves and the corresponding cycle threshold differences. Error bars indicate mean ± s.d. for three technical replicates. *$P < 0.05$; **$P < 0.01$; ***$P < 0.001$; ns, non-significant by t-test (two-tailed).

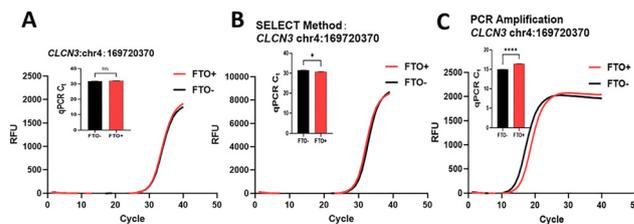

Fig. 4 Comparison of the detection performance between the method developed in this study and the SELECT method for m⁶A sites in the low-abundance transcript CLCN3. Real-time fluorescence amplification curves of our method (A) and SELECT (B). (C) Real-time fluorescence amplification curves of our method after PCR amplification. Error bars indicate mean ± s.d. for three technical replicates. *$P < 0.05$; **$P < 0.01$; ***$P < 0.001$; ns, non-significant by t-test (two-tailed).

validating the enzymatic activity of FTO (Fig. S5 and S6), our method detected specific m⁶A sites on rRNA, lncRNA, and mRNA by monitoring relative ligation product yields before and after FTO-mediated demethylation. In HeLa cells, the method accurately identified the known m⁶A site at 28S rRNA 4190 (Fig. 3A), while no significant change was observed at 18S rRNA A1835 after input normalization (Fig. 3C). Similarly, it successfully detected the known m⁶A site 2577 but not the A site 2511 on lncRNA MALAT1 (Fig. 3B and D). GAPDH served as an internal reference for input normalization throughout.

Subsequently, we selected candidate m⁶A sites from published sequencing data for experimental validation.[30] By comparing the normalized C_t differences between FTO-treated and untreated samples, we confirmed m⁶A presence at multiple sites on tRNA and mRNA[26] (e.g., TRNAK-CUU, IGFBP5, PPRC1; Fig. S8). These results validate both the existence of these sites modification and the broad applicability of our method for locus-specific m⁶A detection across diverse RNA types.

To evaluate our method's performance for low-abundance transcripts, we selected the low-expression mRNA CLCN3 (TPM 13) (TPM stands for Transcripts Per Million, a normalized unit that quantifies gene expression levels[38]). Using approximately 10 ng of cDNA input, we could not reliably detect the reported m⁶A site in CLCN3[25] (Fig. 4A). We attribute this failure to substantial transcript loss during FTO treatment coupled with low transcript abundance. Then we compare our method with SELECT, a widely used approach for detecting m⁶A modifications due to its simplicity and flexibility. Notably, the SELECT method also failed to detect this site under same amount of RNA input (Fig. 4B). However, after amplifying the target cDNA by 35-cycle PCR, our method successfully confirmed the m⁶A site on CLCN3 (Fig. 4C). The SELECT method exploits the difference in steric hindrance between m⁶A and A in RNA to mediate template-driven probe ligation, enabling m⁶A detection. Although RNA is difficult to amplify and not directly compatible with PCR due to DNA polymerases' template

specificity, our approach employs chemical treatment followed by reverse transcription to convert modification information into sequence differences in cDNA. Using cDNA as the substrate for ligation-based detection allows compatibility with PCR amplification, thereby enhancing signal from limited RNA input. For a fair comparison, both methods were assessed under identical conditions, starting with equal amounts of input RNA before processing. The experimental results also indicate a clear advantage over SELECT for low-abundance transcripts and highlights the utility of our approach when sample material is limited.

We next compared METTL3⁺/⁻ HeLa cells with wild-type controls, as METTL3 knockdown reduces global m⁶A levels. After knocking out the METTL3, the degree of methylation at some sites changed. Through our method, such changes can be detected. Western blot confirmed markedly lower METTL3 protein in METTL3⁺/⁻ cells (Fig. 5A, the uncropped images were provided in the Fig. S9).

To control for RNA input variation, samples were normalized by transcript abundance, validating 28S rRNA A4194 sites and lncRNA MALAT1 A2511 in HeLa cells. Following normalization, no significant difference in qPCR C_t values was observed between METTL3⁺/⁻ cells and wild-type cells for these A sites (Fig. 5B and C). We then validated several previously reported m⁶A sites (in IGFBP5, xist, RRP12, TPGS2 and USP47) from sequencing datasets.[26] Ligation product yields at these sites were consistently lower in METTL3⁺/⁻ cells than in wild-type controls (Fig. 5D, E and Fig. S10), confirming them as m⁶A modification sites in HeLa cells.

To assess the method's performance for low-abundance transcripts, we selected three low-expression gene loci and successfully detected m⁶A modifications (Fig. S11). For the low-expression transcript CLCN3, a serial mRNA dilution was performed; after reverse transcription and 35-cycle PCR amplification, m⁶A was consistently detected with inputs as low as 0.02 ng (Fig. 6). These results confirm the method's applicability for samples with limited transcript abundance. We assessed the detection threshold using model oligonucleotides with varying m⁶A ratios. As shown in Fig. S12, the method detected m⁶A levels as low as 20%, with a 2.12 ΔC_t relative to
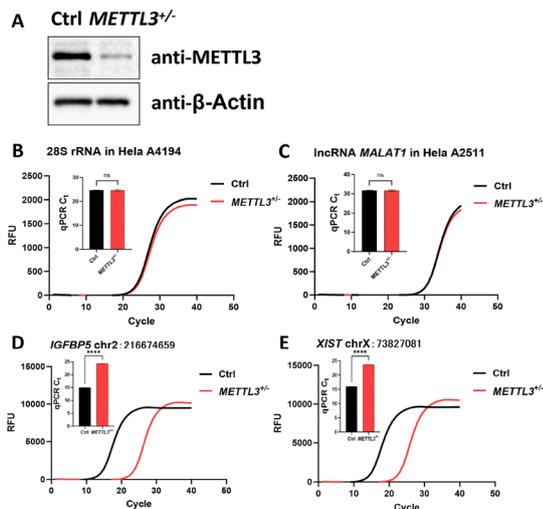
Fig. 5 Detection of m⁶A sites and A sites in RNA from *METTL3*⁺/⁻ HeLa cells and wild-type controls. (A) Western blotting showing that the METTL3 protein level is reduced in *METTL3*⁺/⁻ HeLa heterozygous cells. (B) and (C) Detection results of A sites. (D) and (E) Detection results of m⁶A sites. Error bars indicate mean ± s.d. for three technical replicates. *$P < 0.05$; **$P < 0.01$; ***$P < 0.001$; ns, non-significant by t-test (two-tailed).
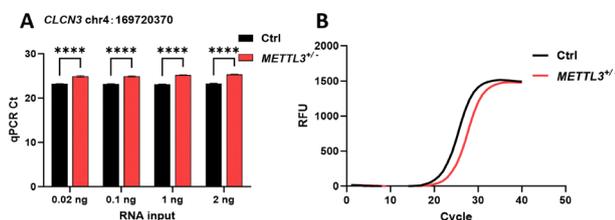

Fig. 6 Comparison minimal mRNA input require for detecting the m6A site in *CLCN3*. (A) qPCR C_t varies under different mRNA inputs. (B) Real-time fluorescence amplification curves of 0.02 ng mRNA input. Error bars indicate mean ± s.d. for three technical replicates. *$P < 0.05$; **$P < 0.01$; ***$P < 0.001$; ns, non-significant by t-test (two-tailed).

the unmodified control, corresponding to a 4.36-fold difference in ligation product abundance.

In summary, we developed a locus-specific m⁶A detection method and successfully identified m⁶A sites in various RNA types, including rRNA, lncRNA, and mRNA. Our method converts modification information into sequence differences in cDNA *via* chemical transformation and reverse transcription. Using amplifiable cDNA as the template enables sensitive detection even with low RNA input. Although the chemical treatment reduces sequence complexity and may limit target selection, the method provides a practical framework for detecting RNA modifications in rare biological samples and, with probe redesign, could be extended to other RNA modifications.

Conflicts of interest

There are no conflicts to declare.

Data availability

The data that support the findings of this study are available in the supplementary information (SI) of this article. Supplementary information is available. See DOI: https://doi.org/10.1039/d6cc00494f.

Acknowledgements

References

1 F. F. Davis and F. W. Allen, *J. Biol. Chem.*, 1957, **227**, 907–915.
2 P. Boccaletto, F. Stefaniak, A. Ray, A. Cappannini, S. Mukherjee, E. Purta, M. Kurkowska, N. Shirvanizadeh, E. Destefanis, P. Groza, G. Avşar, A. Romitelli, P. Pir, E. Dassi, S. G. Conticello, F. Aguilo and J. M. Bujnicki, *Nucleic Acids Res.*, 2022, **50**, D231–D235.
3 J. Liu, Y. Yue, D. Han, X. Wang, Y. Fu, L. Zhang, G. Jia, M. Yu, Z. Lu, X. Deng, Q. Dai, W. Chen and C. He, *Nat. Chem. Biol.*, 2013, **10**, 93–95.
4 G. Jia, Y. Fu, X. Zhao, Q. Dai, G. Zheng, Y. Yang, C. Yi, T. Lindahl, T. Pan, Y.-G. Yang and C. He, *Nat. Chem. Biol.*, 2011, **7**, 885–887.
5 G. Zheng, J. A. Dahl, Y. Niu, P. Fedorcsak, C.-M. Huang, C. J. Li, C. B. Vågbø, Y. Shi, W.-L. Wang, S.-H. Song, Z. Lu, R. P. G. Bosmans, Q. Dai, Y.-J. Hao, X. Yang, W.-M. Zhao, W.-M. Tong, X.-J. Wang, F. Bogdan, K. Furu, Y. Fu, G. Jia, X. Zhao, J. Liu, H. E. Krokan, A. Klungland, Y.-G. Yang and C. He, *Mol. Cell*, 2013, **49**, 18–29.
6 I. A. Roundtree, G.-Z. Luo, Z. Zhang, X. Wang, T. Zhou, Y. Cui, J. Sha, X. Huang, L. Guerrero, P. Xie, E. He, B. Shen and C. He, *eLife*, 2017, **6**, e31311.
7 Q. Zhang, S. Zhao, C. Su, Q. Han, Y. Han, X. Tian, Y. Li and C.-Y. Zhang, *Anal. Chem.*, 2023, **95**, 13201–13210.
8 W.-j Liu, L.-y Wang, Z. Sheng, B. Zhang, X. Zou and C.-y Zhang, *Biosens. Bioelectron.*, 2023, **240**, 115645.
9 C. Zhang, Y. Chen, B. Sun, L. Wang, Y. Yang, D. Ma, J. Lv, J. Heng, Y. Ding, Y. Xue, X. Lu, W. Xiao, Y.-G. Yang and F. Liu, *Nature*, 2017, **549**, 273–276.
10 Y. Xiang, B. Laurent, C.-H. Hsu, S. Nachtergaele, Z. Lu, W. Sheng, C. Xu, H. Chen, J. Ouyang, S. Wang, D. Ling, P.-H. Hsu, L. Zou, A. Jambhekar, C. He and Y. Shi, *Nature*, 2017, **543**, 573–576.
11 H. Shi, X. Zhang, Y.-L. Weng, Z. Lu, Y. Liu, Z. Lu, J. Li, P. Hao, Y. Zhang, F. Zhang, Y. Wu, J. Y. Delgado, Y. Su, M. J. Patel, X. Cao, B. Shen, X. Huang, G.-L. Ming, X. Zhuang, H. Song, C. He and T. Zhou, *Nature*, 2018, **563**, 249–253.
12 R. Winkler, E. Gillis, L. Lasman, M. Safra, S. Geula, C. Soyris, A. Nachshon, J. Tai-Schmiedel, N. Friedman, V. T. K. Le-Trilling, M. Trilling, M. Mandelboim, J. H. Hanna, S. Schwartz and N. Stern-Ginossar, *Nat. Immunol.*, 2018, **20**, 173–182.
13 D. Dominissini, S. Moshitch-Moshkovitz, S. Schwartz, M. Salmon-Divon, L. Ungar, S. Osenberg, K. Cesarkas, J. Jacob-Hirsch, N. Amariglio, M. Kupiec, R. Sorek and G. Rechavi, *Nature*, 2012, **485**, 201–206.
14 K. D. Meyer, Y. Saletore, P. Zumbo, O. Elemento, C. E. Mason and S. R. Jaffrey, *Cell*, 2012, **149**, 1635–1646.
15 B. Linder, A. V. Grozhik, A. O. Olarerin-George, C. Meydan, C. E. Mason and S. R. Jaffrey, *Nat. Methods*, 2015, **12**, 767–772.
16 K. Chen, Z. Lu, X. Wang, Y. Fu, G. Z. Luo, N. Liu, D. Han, D. Dominissini, Q. Dai, T. Pan and C. He, *Angew. Chem., Int. Ed.*, 2014, **54**, 1587–1590.
17 C. W. Q. Koh, Y. T. Goh and W. S. S. Goh, *Nat. Commun.*, 2019, **10**, 5636.
18 X. Shu, J. Cao, M. Cheng, S. Xiang, M. Gao, T. Li, X. Ying, F. Wang, Y. Yue, Z. Lu, Q. Dai, X. Cui, L. Ma, Y. Wang, C. He, X. Feng and J. Liu, *Nat. Chem. Biol.*, 2020, **16**, 887–895.
19 L. Hu, S. Liu, Y. Peng, R. Ge, R. Su, C. Senevirathne, B. T. Harada, Q. Dai, J. Wei, L. Zhang, Z. Hao, L. Luo, H. Wang, Y. Wang, M. Luo, M. Chen, J. Chen and C. He, *Nat. Biotechnol.*, 2022, **40**, 1210–1219.

20 K. Hartstock, N. A. Kueck, P. Spacek, A. Ovcharenko, S. Hüwel, N. V. Cornelissen, A. Bollu, C. Dieterich and A. Rentmeister, *Nat. Commun.*, 2023, **14**, 7154.

21 Y. Wang, Y. Xiao, S. Dong, Q. Yu and G. Jia, *Nat. Chem. Biol.*, 2020, **16**, 896–903.

22 M. A. Garcia-Campos, S. Edelheit, U. Toth, M. Safra, R. Shachar, S. Viukov, R. Winkler, R. Nir, L. Lasman, A. Brandis, J. H. Hanna, W. Rossmanith and S. Schwartz, *Cell*, 2019, **178**(731–747), e716.

23 H.-X. Chen, Z. Zhang, D.-Z. Ma, L.-Q. Chen and G.-Z. Luo, *Methods*, 2022, **203**, 392–398.

24 K. D. Meyer, *Nat. Methods*, 2019, **16**, 1275–1280.

25 Y.-L. Xiao, S. Liu, R. Ge, Y. Wu, C. He, M. Chen and W. Tang, *Nat. Biotechnol.*, 2023, **41**, 993–1003.

26 C. Liu, H. Sun, Y. Yi, W. Shen, K. Li, Y. Xiao, F. Li, Y. Li, Y. Hou, B. Lu, W. Liu, H. Meng, J. Peng, C. Yi and J. Wang, *Nat. Biotechnol.*, 2022, **41**, 355–366.

27 H. Sun, B. Lu, Z. Zhang, Y. Xiao, Z. Zhou, L. Xi, Z. Li, Z. Jiang, J. Zhang, M. Wang, C. Liu, Y. Ma, J. Peng, X.-J. Wang and C. Yi, *Nat. Methods*, 2025, **22**, 1226–1236.

28 P. Wang, C. Ye, M. Zhao, B. Jiang and C. He, *Nat. Chem.*, 2025, **17**, 1042–1052.

29 N. Liu, M. Parisien, Q. Dai, G. Zheng, C. He and T. Pan, *RNA*, 2013, **19**, 1848–1856.

30 Y. Xiao, Y. Wang, Q. Tang, L. Wei, X. Zhang and G. Jia, *Angew. Chem., Int. Ed.*, 2018, **57**, 15995–16000.

31 Y. Wang, Z. Zhang, C. Sepich-Poore, L. Zhang, Y. Xiao and C. He, *Angew. Chem., Int. Ed.*, 2020, **60**, 873–880.

32 F. Su, W. Liu, K. Gao, D. Chen, Y. Cheng and Z. Li, *Anal. Chim. Acta*, 2024, **1302**, 342474.

33 J. Li, J. Zhou, Y. Xia, Y. Rui, X. Yang, G. Xie, G. Jiang and H. Wang, *Nucleic Acids Res.*, 2023, **51**, e51.

34 Q. Zhang, Y. Dai, X. Teng and J. Li, *Angew. Chem., Int. Ed.*, 2024, **64**, e202420977.

35 X. Ren, R. Deng, K. Zhang, Y. Sun, Y. Li and J. Li, *Angew. Chem., Int. Ed.*, 2021, **60**, 22646–22651.

36 M. Song, J. Wang, J. Hou, T. Fu, Y. Feng, W. Lv, F. Ge, R. Peng, D. Han and W. Tan, *ACS Nano*, 2024, **18**, 27537–27546.

37 H.-J. Li, J. Hu, W.-J. Liu and C.-Y. Zhang, *TrAC, Trends Anal. Chem.*, 2026, **194**, 118537.

38 G. P. Wagner, K. Kin and V. J. Lynch, *Theory Biosci.*, 2012, **131**, 281–285.